SUPPLEMENTARY INFORMATION

1. *Deeper penetration of diving vessels*

In the manuscript, we pointed flow reorganization across different cortical layers after chronic cocaine exposures. Fig.s1 shows the MIP images (x-z plane) after 32 days of cocaine treatment vs its baseline (Day 0) showing increased diving path and enhanced flow in deep cortical layers (300-600µm). The baseline image (a) barely shows diving vessels beyond 600µm; In contrast, flow is readily detectable after Day 32 of cocaine treatment even beyond 600µm as pointed by white arrows. The longer vessels or faster flow implies that cocaine associated flow increase routs to deeper cortical layers as an effect of increasing collateral flow to compensate for local flow or metabolic deficits needed for neuronal activity.

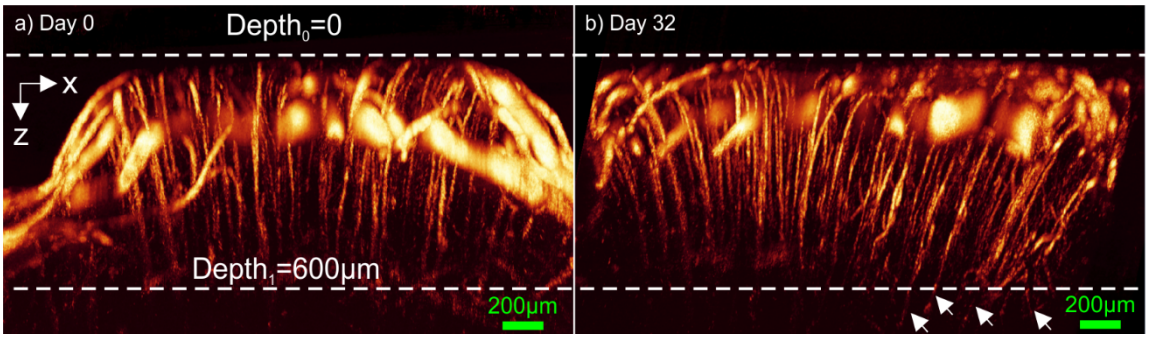

Fig.s1 Increased depth of penetrating vessels after chronic cocaine treatment. a) and b) are MIP images (x-z plane) of 3D µODT to show cerebral vascular networks in mouse sensorimotor cortex on Day 0 (baseline) and on Day 32 after chronic cocaine exposures, respectively. White arrows point out the deeper diving vessels due to the flow reorganization which are missing on Day 0.

2. *Microvascular network segmentation*

To segment binary vascular networks from µOCA images, we applied a hybrid approach combining Frangi-Hessian method [4] with region grow algorithm, in which Frangi-Hessian and region grow methods segment microvascular network and large branches, respectively. Briefly, Frangi-Hessian filter calculates the vessel-likeness of individual pixel x_0 in a 2D/3D image by analyzing eigenvalues (λ_1, λ_2, λ_3) of Hessian matrix applied on the original image. Taking the assumption of $|\lambda_1| \leq |\lambda_2| \leq |\lambda_3|$, the smallest eigenvalue λ_1 corresponds to the vessel orientation ($\lambda_1 \rightarrow 0$) and λ_2, λ_3 are eigenvalues in the radial directions. In a 3D image, eigenvalues of a tubular structure satisfy $|\lambda_1| \approx 0$, $|\lambda_1| << |\lambda_2|$, $\lambda_2 \approx \lambda_3$. To calculate the vessel likeness of a tubular structure in 2D, a geometric ratio (R_B) and magnitude factor (S) were defined,

$$R_B = \frac{|\lambda_1|}{|\lambda_2|} \; and \; S = \sqrt{\lambda_1^2 + \lambda_2^2} \qquad \text{(s1)}$$

Then, the vessel-likeness of a tubular structure in a 2D image can be calculated by

$$2D: \quad v_0(s) = \begin{cases} 0 & if\ \lambda_2 > 0\ or\ \lambda_3 > 0 \\ \exp\left(-\frac{R_B^2}{2\beta^2}\right)\left(1-\exp\left(-\frac{S^2}{2c^2}\right)\right) \end{cases} \qquad \text{(s2)}$$

where β and c are custom thresholding parameters that determine the sensitivity of Frangi-Hessian filtering to tubular shape.

Region grow algorithm is to grow a manually set 'seed' pixel by evaluating the intensity difference between the test pixel I_T in surrounding neighborhood and the 'seed' pixel I_S. When the grey-level difference between the test and the 'seed' pixel is smaller than a given threshold T, we define the test pixel as a new 'seed' pixel. The growing procedure continues and does not stop until no more test pixels could be included in 'seeds' domain.

Fig.s2 illustrates the flow chart of the hybrid segmentation method. Firstly, a seed is manually placed on the big braches to initiate the region grow iteration and to generate a binary mask of large branches (Fig.s2b). At the meantime, a vessel-likeness map of microvasculature (Fig.s2c) is calculated by Frangi-Hessian method with small Hessian matrix (1≤σ≤3). The second step is to binarize vessel-likeness map of microvasculature (Fig.s2c) using a rolling adaptive thresholding window (Fig.s3c). After obtaining the binary image of both large branches and microvasculature, two images are merged and yield the binary mask of entire cerebral vascular network (Fig.s3e).

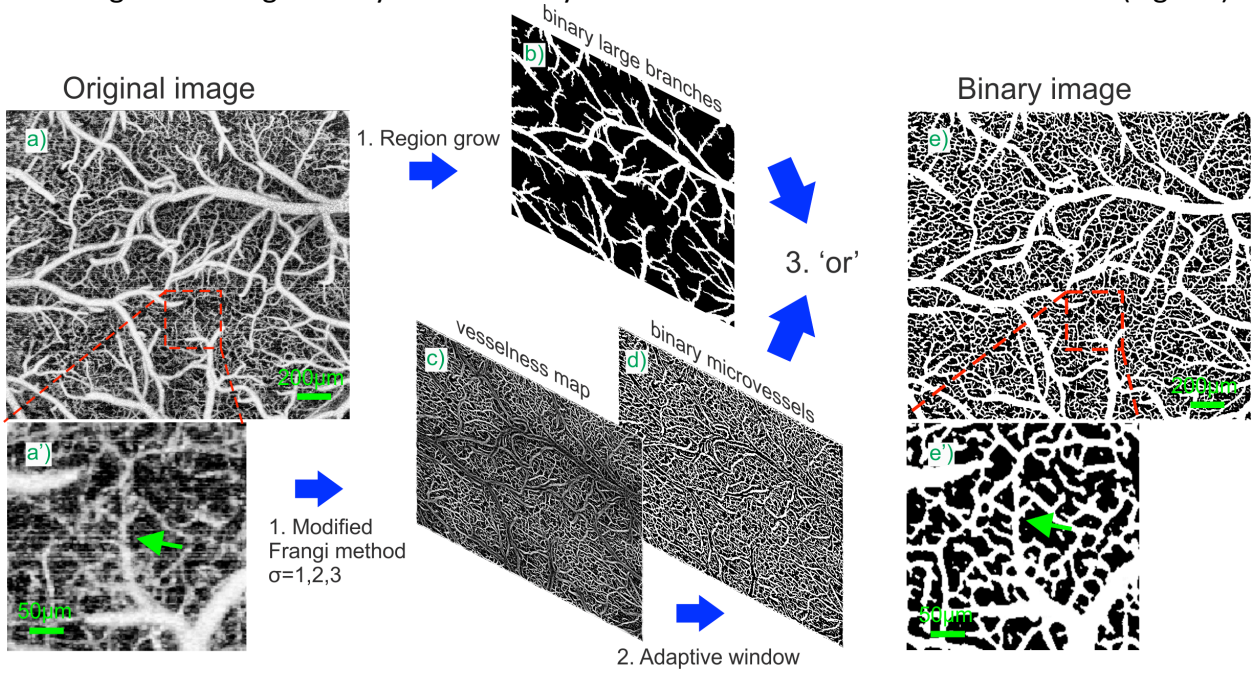

Fig.s2 Flow chart of hybrid segmentation combining Frangi-Hessian method and region grow algorithm. a) and a'): Original μOCA image of mouse sensorimotor cortex and the zoom-in image of ROI (red dashed box). b) Binary image of large branches by region grow algorithm; c) Vessel-likeness map calculated by Frangi-Hessian filter of small scale (σ=1, 2, 3); d) Binary image of the

microvasculature. e) and e'): Binary image of entire vascular network and the zoom-in image of ROI (red dashed box). Green arrows in a') and e') point out the uncovered microvascular details.

3. Spatial resolved microvascular density map of full-thickness cortex

To extract the microvascular networks from the vascular tree, diameter thresholds are applied to classify vascular networks according to their diameters (Fig.s3g). Fig.s3 is the flow chart for generating diameter coded skeleton image. Fig.s3b is the binary mask of vascular network generated by our hybrid method and Fig.s3c is the inverted mask. Then the skeleton image (Fig.s3d) and Euclidean distance map (Fig.s3e) which characterizes vessel diameters were calculated based on Fig.s3b and Fig.s3c, respectively. Finally, the diameter coded skeleton can be obtained by 'point to point' multiplication between Fig.s3d and Fig.s3e. After thresholding, the skeleton image corresponding to certain diameter range was binarized again for density measurement.

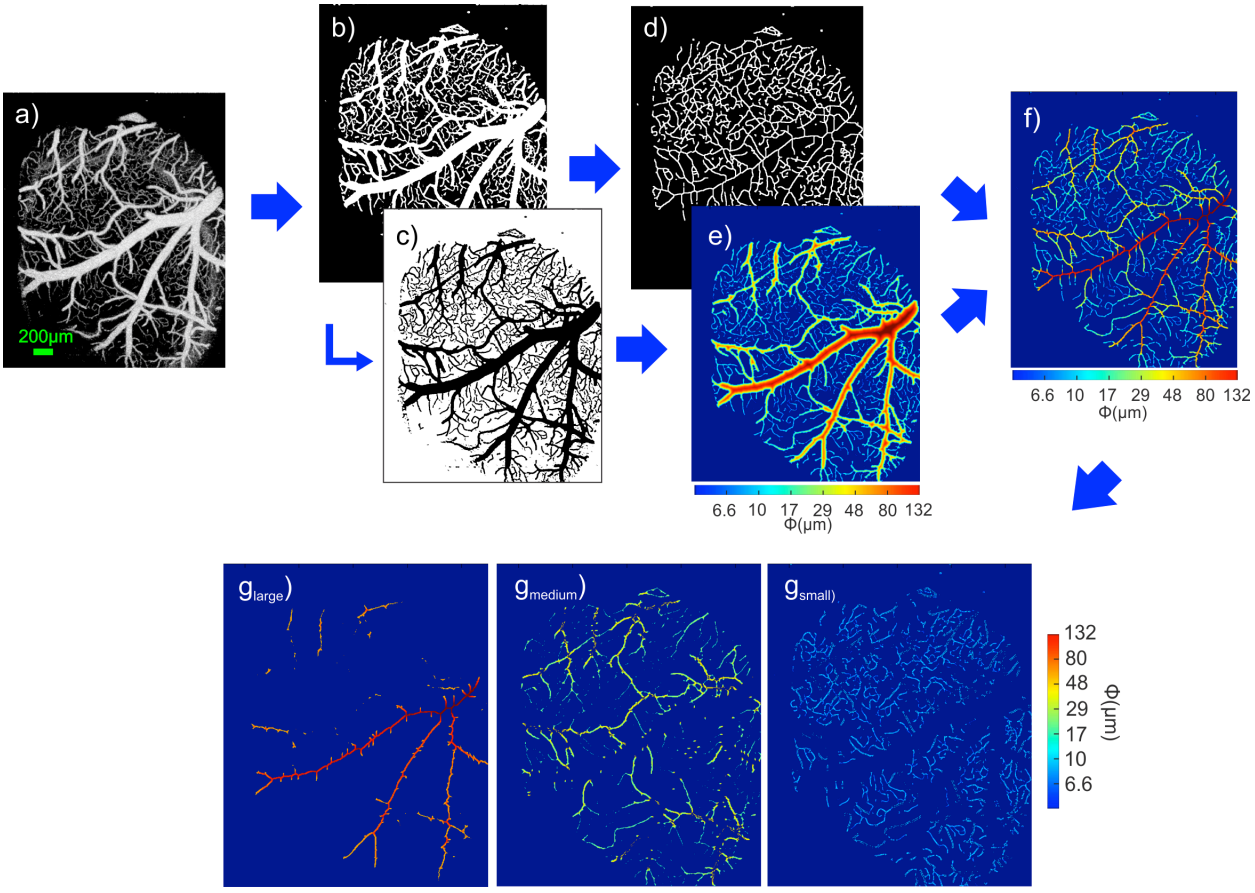

Fig.s3 Flow chart for classifying vascular networks of different diameter range in a thin cortical layer (e.g. 100µm of thickness) a) Original µOCA MIP image of vascular network of a thin cortical layer, b) Binary image by hybrid method, c) Inverted binary image of b), d) Skeleton image, e) Euclidean distance map, f) Skeletonized Euclidean distance map, and g_{large}), g_{medium}), g_{small}) are

segmented vessel skeletons of large ($\phi \geq 40\mu m$), medium ($16\mu m \leq \phi \leq 40\mu m$) and small ($\phi \leq 16\mu m$) vessels.

A full-thickness 3D μOCA image of mouse cortex (600μm) is sectioned into 6 sub-volumetric μOCA images, yielding 6 microvascular skeleton images (Fig. s4b). Then the microvascular skeleton of upper (0-300μm) and bottom (300-600μm) cortex can be obtained by taking the maximum intensity projection of the corresponding layers (0-300μm: MIP of layer 1-3, 300-600μm: MIP of layer 4-6). To generate the density map, an adaptive rolling window method (window size: W×W, W=60 pixels) is utilized to calculate vascular density fraction, or fill factor (FF) which characterizes the density level of the target window. Then FF is assigned to each individual pixel covered by the rolling window to generate a spatial resolved density map.

$$FF = \frac{Total\ vessel\ pixel\ \#}{Total\ pixel\ \#\ of\ ROI} \tag{s3}$$

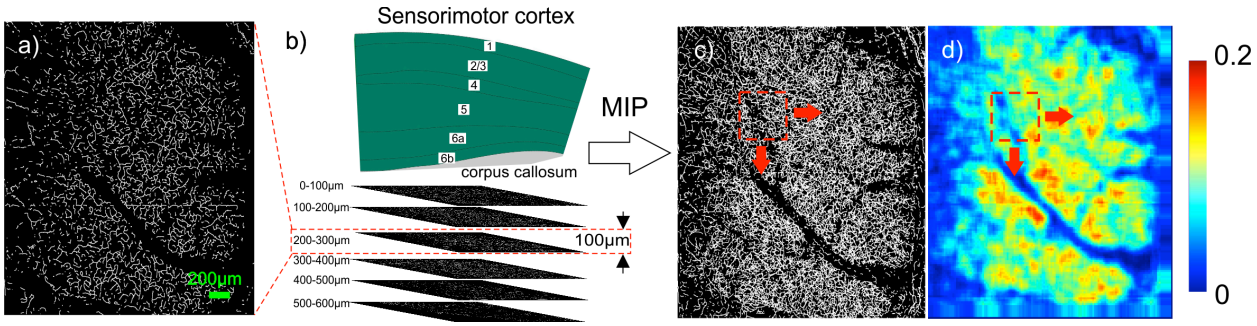

Fig.s4 Calculation of spatial resolved density map a) Skeleton of microvasculature ϕ_T<16μm of a single cortical layer b) 6 subsections of a full-thickness cortex c) MIP image of skeleton images of the first 3 cortical layers (0-300μm) d) Spatial resolved density map of MIP skeleton image c). Red dashed square represents the adaptive window and the red arrows show its rolling direction.

4. Ultrahigh-resolution optical coherence tomography (μOCT)

A custom μOCT system was used for ultrahigh-resolution optical coherence angiography (μOCA) and optical Doppler tomography (μODT), which enabled capillary-resolution imaging of 3D cerebral vasculature (μOCA) and flow networks (μODT) by decoding the spectral fringes backscattered from the sample and the reference arms. Briefly, the μOCT setup was powered by an ultra-broadband superluminescence diode (λ_0=1310nm, $\Delta\lambda_{FWHM}$=200nm) whose output light illuminated a 2×2 wideband monomode fiberoptic coupler. The reference light was reflected by stationary mirror after passing through a prism pair for dispersion compensation. Light exiting the sample arm was collimated to ~ϕ5mm and focused by an achromatic lens (f18mm/NA0.25) on the capillary beds under the surface of mouse's somatosensory cortex through a cranial window. The backscattered light (along z-axis) was collected by the same optics path back to the sample arm and interfered with the reference light in the detection fiber. The recombined light passed through a custom high-throughput spectrometer (Wasatch photonics), whose spectral

components, including spectral interference fringes, were evenly projected onto a linear InGaAs array (GL2048, Sensors Unlimited) with a highest line rate of 147kHz. For the system setup, an axial resolution (defined by the coherence length $L_c=2ln2/\pi\cdot\lambda^2/\Delta\lambda_{cp}$) of ~2.8μm and a lateral resolution of ~3.2μm were reached in brain tissue. The Doppler velocity was retrieved by measuring the phase difference $\Delta\phi_{z,x}$ between adjacent A-scans, which were calculated by either the phase subtraction method *(PSM) as* $v_{z,x}=\lambda\Delta\phi_{z,x}/(4\pi n\tau\cos\vartheta)$*, where* θ_z *is the angle between blood flow and the light incidence, n is refractive index of tissue and* τ *is time interval between 2 adjacent A-scans, or by the phase intensity method (PIM)[1]*. As the process was computationally intensive, graphic processing unit (GPU) was implemented to boost both FFT and PSM or PIM reconstruction, allowing for real-time rendering (e.g. 473fps 1k×2k pixels B-scan) and instantaneous display of maximum intensity project (MIP) [2, 3].

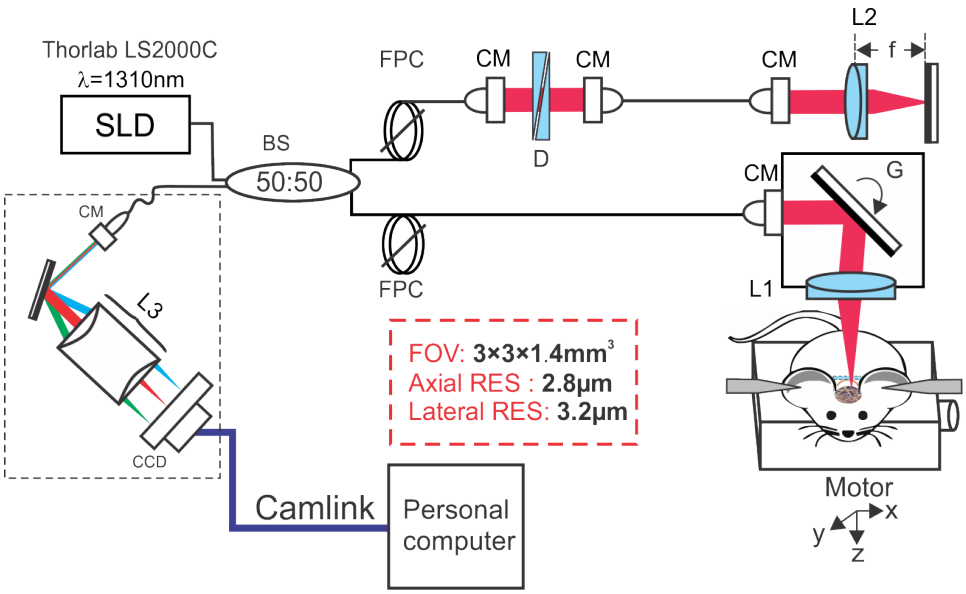

Fig.s5 Schematic diagram of the μODT system. SLD: superluminescence diode, BS: beam splitter, CM: Collimator, FPC: Polarization controller, G: Galvo scanner L1: Sample arm objective, L2: Reference arm lens, L3: Detector lens group, D: dispersion compensation prism pairs.

Reference

1. H.-G. Ren, C.-W. Du, Z.-J. Yuan, K. Park, N. D. Volkow, and Y.-T. Pan,Mol Psychiatry **17**, 1017-1025 (2012).
2. J. You, Q. Zhang, K. Park, C. Du, and Y. Pan,Opt. Lett. **40**, 4293-4296 (2015).
3. J. You, C. Du, N. D. Volkow, and Y. Pan,Biomed. Opt. Express **5**, 3217-3230 (2014).
4. Y. Sato, S. Nakajima, N. Shiraga, H. Atsumi, S. Yoshida, T. Koller, G. Gerig, and R. Kikinis,Medical Image Analysis **2**, 143-168 (1998).